Submitted to ApJ, 2005 Oct. 21; Revised 2005 Dec. 23 and 2006 Jan. 20

The Albedo, Size, and Density of Binary Kuiper Belt Object (47171) 1999 TC_{36}

J.A. Stansberry[1]

stansber@as.arizona.edu

W.M. Grundy[2]

J.L. Margot[3]

D.P. Cruikshank[4]

J. P. Emery[5]

G.H. Rieke[1]

D.E. Trilling[1]

ABSTRACT

We measured the system-integrated thermal emission of the binary Kuiper Belt Object (47171) 1999 TC_{36} at wavelengths near 24 and 70 μm using the *Spitzer* space telescope. We fit these data and the visual magnitude using both the Standard Thermal Model and thermophysical models. We find that the effective diameter of the binary is 405 km, with a range of 350 – 470 km, and the effective visible geometric albedo for the system is 0.079 with a range of 0.055 – 0.11. The binary orbit, magnitude contrast between the components, and system mass have been determined from HST data (Margot et al., 2004; 2005a; 2005b). Our effective diameter, combined with that system mass, indicate an average

[1]University of Arizona, Tucson, AZ 85721

[2]Lowell Observatory, Flagstaff, AZ 86001

[3]Cornell University, Ithaca, NY 14853

[4]NASA Ames Research Center, Moffett Field, CA 94035

[5]SETI Institute, Mountain View, CA 94043

density for the objects of 0.5 g/cm^3, with a range 0.3 – 0.8 g/cm^3. This density is low compared to that of materials expected to be abundant in solid bodies in the trans-Neptunian region, requiring 50 – 75% of the interior of (47171) 1999 TC_{36} be taken up by void space. This conclusion is not greatly affected if (47171) 1999 TC_{36} is "differentiated" (in the sense of having either a rocky or just a non-porous core). If the primary is itself a binary, the average density of that (hypothetical) triple system would be in the range 0.4 – 1.1 g/cm^3, with a porosity in the range 15 – 70%.

Subject headings: Kuiper Belt Objects: general — Kuiper Belt Objects: individual((47171) 1999 TC36) — Kuiper Belt Objects: infrared observations — small bodies: binaries

1. Introduction

The physical properties of Kuiper Belt Objects (KBOs) remain poorly known 13 years after the discovery of the first KBO, (15760) 1992 QB_1 (Jewitt and Luu, 1993). While they can be discovered, their orbits determined, and their visible-light colors measured (to some extent) using modest telescopes, learning more about KBOs generally requires the largest of ground-based telesopes, or space-based instrumentation. The *Hubble Space Telescope* (HST) has revealed that the Kuiper Belt hosts a large population of binary systems (*e.g.* Noll, 2003). Currently 21 KBOs are known to be binary (Veillet *et al.* 2002; Elliot *et al.* 2001; Noll *et al.* 2002a, 2002b, 2002c; Millis & Clancy 2003; Stephens & Noll, 2004; Stephens and Noll, 2005; Cruikshank *et al.* 2005). Very recently, two new moons were discovered in the Pluto-Charon system (Weaver *et al.* 2005; Buie *et al.* 2005), making it a quadruple, and the large KBO 2003 EL_{61} has been shown to have 2 moons, making it a triple (Brown *et al.* 2005).

Stephens and Noll (2005) find that of the 81 KBOs they observed with HST/NICMOS, 11% are binary (at current detection limits). They also suggest find that objects with very low inclinations and eccentricities ("cold-classical" objects) are likely to be binary at a rate of 21%, while other, dynamically hotter classes, are binary at a rate of 6%. The high incidence of binarity among KBOs is of considerable intrinsic interest as a probe of the dynamics of the Kuiper Belt (*e.g.* Stern, 2002; Goldreich *et al.* 2002; Astakhov *et al.* 2005). However, binaries are also of particular interest because their masses can be determined from observations of the relative motions of the components. Such measurements would otherwise be impossible without sending a spacecraft. When combined with measurements of sizes, the masses of primitive solar system objects can be used to constrain their density. The densities of KBOs

are indicative of their interior structure, and can provide clues to the composition of and conditions in the outermost primitive solar nebula.

Spitzer (Werner *et al.* 2004) offers unique capabilities for measuring the infrared emission from KBOs and other solar system objects, thereby constraining their albedos and sizes (*e.g.* Stansberry *et al.* 2004; Cruikshank *et al.* 2004; Lisse *et al.* 2005). (47171) 1999 TC_{36} and three other KBOs have been detected in the sub-millimeter (Altenhoff *et al.* 2004; Margot *et al.* 2002; Lellouch *et al.* 2002; Jewitt *et al.* 2001; see also Grundy *et al.* 2005). One KBO, Quaoar, has been resolved at optical wavlengths, providing an estimate of its size (Brown and Trujillo 2004). For KBOs, the Multiband Imaging Photometer for *Spitzer* (MIPS), with photometry channels near 24, 70, and 160 μm, covers the peak in the typical spectral energy distribution near 80 μm. Measurements at these wavelengths are sensitive to the distribution of temperature across the surface of a KBO, and so can reveal something about the thermal properties of near-surface layers as well as constraining the size and albedo of the target.

1.1. (47171) 1999 TC_{36}

Here we report on our *Spitzer* observations of the binary KBO (47171) 1999 TC_{36}, the albedo and size that are indicated by those data, and the density we derive by combining our results with the *Hubble Space Telescope* (HST) visible-imaging results of Margot *et al.* (2004; 2005a; 2005b). (47171) 1999 TC_{36} orbits in the 3:2 resonance with Neptune, and so likely formed closer to the Sun than its current semi-major axis would suggest (*e.g.* Malhotra, 1993). It is very red, with $B - V \simeq 1.05$, $V - R \simeq 0.70$ (Dotto *et al.* 2003; Doressoundiram *et al.* 2005) and $V - J \simeq 2.3$ (Dotto *et al.* 2003; McBride *et al.* 2003). Lazzarin *et al.* (2003) and Dotto *et al.* (2003) give visible to near-IR spectra, and Dotto suggests a combination of tholins, carbon and water ice as a plausible surface composition. There appears to be some slight confusion as to the absolute magnitude, H_V, of this object. Both the IAU Minor Planet Center (MPC, http://cfa-www.harvard.edu/iau/mpc.html) and the Solar System Dynamics Division at the Jet Propulsion Laboratory (Horizons, http://ssd.jpl.nasa.gov/horizons.html) give values of $H_V < 5$, presumably based on apparent magnitudes from astrometric observations. Photometric studies of (47171) 1999 TC_{36} all conclude that H_V is in the range 5.33 – 5.55 (Margot *et al.* 2005a; 2005b; Tegler and Romanishin 2005; Doressoundiram *et al.* 2005; McBride *et al.* 2003, Delsanti *et al.* 2001; Boehnhardt *et al.* 2001). Here we adopt the value of Doressoundiram *et al.* (2005), $H_V = 5.37 \pm 0.05$, as representative of the range of H_V. The $\leq 5\%$ scatter in the H_V determinations by different groups is small relative to the photometric errors of our *Spitzer* measurements, so we do not track its quite small contribution to the uncertainties in our results. (We also note a systematic bias between

the MPC and Horizons absolute magnitudes, and absolute magnitudes found in dedicated photometric surveys, as detailed by Tegler and Romanishin (2005).)

Trujillo and Brown (2002) identified (47171) 1999 TC_{36} as a binary, with a separation of about 8000 km. Margot *et al.* (2005a; 2005b) imaged the binary with HST over a period of 25 months, determining the system's orbital period, semi-major axis, and total mass, to high precision. Table 1 summarizes the heliocentric orbit of (47171) 1999 TC_{36}, and the binary parameters of the system as determined in that study. In their PSF and orbital fits for (47171) 1999 TC_{36}, Margot et al found that the residuals were significantly higher than for other binaries in their sample, a finding that can possibly be attributed to the primary being itself a binary, an idea we return to later

2. Observations and Data Analysis

We observed (47171) 1999 TC_{36} with the Multiband Imaging Photometer for *Spitzer* (MIPS, Rieke *et al.* 2004) in its 24 and 70 μm bands, which have effective wavelengths of 23.68 and 71.42 μm. Data were collected using the photometry observing template, which is tailored for photometry of point sources. The telescope tracked the target during the observations, although the motion was negligible relative to the size of the *Spitzer* point-spread function (PSF) at these wavelengths. In photometry mode images of the target are taken at many dithered positions on the arrays to improve the photometric accuracy and the sampling of the PSF. Photometric repeatability on moderately bright sources is better than 2% at 24 μm, and is 5% at 70 μm. The uncertainty in the absolute calibration of these bands is 5% and 15% respectively. For purposes of fitting models to our photometry, we use uncertainties that are the root-square-sum of the absolute calibration uncertainties and the measurement uncertainties determined from the images themselves. The widths of the filter bandpasses are about 25%, resulting in modest color corrections. We iteratively applied color corrections to our photometry, which converged to give a color temperature of 64.5 K, and color corrections of +1% and +10% at 24 and 70 μm respectively. The uncertainties on the correction factors are perhaps a few percent of the factors themselves, and so are negligible for our study. Color corrections for the MIPS bands are available from the *Spitzer Science Center* website (http://ssc.spitzer.caltech.edu).

We reduced the raw data and mosaicked them using the MIPS instrument team data analysis tools (Gordon *et al.* 2004). For the 24 μm data basic processing included slope fitting, flat-fielding, and corrections for droop. All of these steps are currently implemented in the *Spitzer Science Center* (SSC) pipeline products. Additional corrections were made to remove readout offset (a jailbar pattern in the images), the effects of scattered light (which

introduces a pointing-dependent background gradient and slightly degrades the sensitivity), and the application of a second-order flat, derived from the data itself, to remove latents from previous observations. These additional processing steps will be incorporated into the SSC pipeline data products by *circa* the end of 2006. For the field where we observed (47171) 1999 TC_{36}, the additional processing reduced the total noise (including both conventional noise and that due to background sources) in the 24 μm image by 30%. The 70 μm data processing was basically identical to that of the *Spitzer* pipeline (version S12). We converted the calibrated instrumental count rates to flux density using factors of 1.042 μJy/$''^2$ and 16.6 mJy/$''^2$ in the 24 and 70 μm bands, respectively. Figure 1 shows the resulting images.

We measured the flux density of (47171) 1999 TC_{36} using apertures $9\farcs96$ and $29\farcs6$ (about 4 and 3 native pixels) in diameter at 24 and 70 μm; the PSF full-width at half-max is $6\farcs5$ and $20''$ in those bands. The apertures were positioned at the center-of-light centroid. These small apertures improve the signal-to-noise ratio of the measurements, but require both excellent sampling of the PSF, and the application of significant aperture corrections. Mosaics were constructed using $1.245''$ and $4.925''$ pixels at 24 and 70 μm (about 1/2 the native pixel scale of those arrays). Mosaicking at this level of sub-sampling, in combination with the multiply-dithered nature of the observations, results in images with excellent PSF sampling and centroid reproducibility. We computed aperture corrections using smoothed STinyTim model PSFs. We smoothed the model PSFs until they agreed with observed stellar PSFs, giving a noiseless, perfectly normalized, zero-background model PSF. We performed photometry on the result, deriving aperture corrections of 1.91 and 1.85 at 24 and 70 μm, respectively. This method has been verified to result in errors $\leq$ 1% in the photometry of calibration stars of moderate brightness. The response of the MIPS detectors is quite linear for signals ranging from the natural sky background to near the saturation limit, so our aperture corrections should apply accurately for photometry of faint sources. Table 2 summarizes the circumstances of our observations and the measured, color-corrected flux densities: 1.23 ± 0.06 and 25.4 ± 4.7 mJy at 24 and 70 μm, respectively.

Because we did not make a second observation of the field where we detected (47171) 1999 TC_{36}, it is impossible to rule out the possibility that a background source may have coincided with our target, biasing our photometry. However, the areal density of extra-galactic sources bright enough to have influenced our results is quite low, and the probability that one could have serendipitously fallen within our beam is quite low in both bands. The areal density of 0.1$\pm$0.05 mJy 24 μm sources is 3 / arcmin^2 (Papovich *et al.* 2004). For our aperture size (0.022 arcmin^2) this translates into a probability of 6.6% that our 24 μm photometry could be contaminated by a 0.1 mJy source. The probability that a fainter source falls in the beam is higher, but such a source would have an insignificant effect on our photometry. We compute the areal density of 70 μm sources based on the results of Dole *et*

al. (2004). At 70 μm the density of 3 ± 1 mJy sources is ~ 0.4/arcmin^2, which translates to an 7.6% probability of a contaminating source in our 0.19 arcmin^2 aperture. Again, fainter sources are more likely than this to fall within the beam, but would have an insignificant effect on the photometry. Thus, not only is the probability of contamination by an extra-galactic source small at relevant flux densities, the effect on our photometry would be small relative to our estimated flux errors. Furthermore, the observed 24 to 70um color is redder than would be expected for a typical background source. For (47171) 1999 TC_{36} the 70:24 ratio of fluxes is ~ 20, whereas the results of Papovich et al. (2004) and Dole et al. (2004), indicate that a typical ratio for a background galaxy is ~ 10. Thus is is unlikely that our photometry is strongly contaminated by a background galaxy, because such contamination would result in an untenably high color temperature, whereas the color temperature we derive (see below) is very plausible for an object at the distance of (47171) 1999 TC_{36}.

Sources within the galaxy can also contaminate far-IR photometry. In particular, thermal emission from extended, uneven clouds of interstellar dust can increase the noise in regions of the sky where such "infrared cirrus" appears in the background. An advantage of *Spitzer* and MIPS over earlier far-IR missions is the relatively small PSF, the fact that the PSF is well-sampled by the pixels, and the fact that the field of view of the arrays is significantly larger than the PSF. These facts allow direct estimation of the contribution of IR cirrus (and extra-galactic confusion for that matter) directly from the images. Inspection of Figure 1 shows that cirrus did not constribute significantly to our photometric errors.

It also seems unlikely that there could be a coma contributing significantly at 24 or 70 μm, because there is no evidence for variability in the visible colors or absolute magnitudes from multiple photometric observations. A possibility that we can not rule out is that (47171) 1999 TC_{36} posesses a coma dominated by relatively large particles that would scatter poorly at visible to near-IR wavelengths, but which could contribute significantly in the thermal. Given the lack of any direct evidence of a coma around (47171) 1999 TC_{36}, and the requirement that it be both IR-bright and V-invisible to affect our interpretation of the data, we do not pursue this possibility further here.

2.1. Thermal Modeling and Results

The Standard Thermal Model (STM, Lebofsky & Spencer 1989) is the most widely used model for interpreting observations of thermal emission from small bodies in the asteroid main belt and the outer Solar System (*c.f.* Tedesco et al. 2002; Fernández et al. 2002; Campins et al. 1994). The model assumes a spherical body whose surface is in instantaneous equilibrium with the insolation, equivalent to assuming either a thermal inertia of zero, a

non-rotating body, or a rotating body illuminated and viewed pole-on. In the STM the subsolar point temperature is

$$T_0 = [S_0(1 - p_V q)/(\eta\epsilon\sigma)]^{1/4} , \quad (1)$$

where S_0 is the solar constant at the distance of the body, p_V is the geometric albedo, q is the phase integral (assumed here to be 0.39, equivalent to a scattering assymetry parameter, $G = 0.15$ (Lumme and Bowell 1981; Bowell *et al.* 1989)), η is the beaming parameter, ϵ is the emissivity (which we set to 0.9), and σ is the Stefan-Boltzmann constant. Given T_0, the temperature as a function of position on the surface is $T = T_0\mu^{1/4}$, where μ is the cosine of the insolation angle. The nightside temperature is taken to be zero. Surface roughness leads to localized variations in surface temperature and non-isotropic thermal emission (beaming) because individual points on the surface radiate their heat preferentially in the sunward direction. Thus, when viewed at small phase angles, rough surfaces appear warmer than smooth ones, and the thermal emission tends to be dominated by emission from the warmer depressions and sunward-facing slopes. This effect is captured by the beaming parameter, η. Lebofsky et al. (1986) found $\eta = 0.76$ for Ceres and Vesta; the nominal range for η is 0 to 1, with unity corresponding to a perfectly smooth surface (Lebofsky & Spencer 1989). In modeling the thermal emission from a large sample of Jovian Trojan asteroids, Fernández *et al.* (2003) found a typical value of η for that population of about 0.94. It is worth noting that η enters the equations for the surface temperature in a manner analogous to the emissivity, so our results could be couched in terms of emissivity rather than beaming parameter.

The thermal emission from a target is calculated by computing a surface integral of the Planck function over the visible portion of the object (because we do this integral, our model is formally a modified version of the STM). The Planck function at a particular point on the surface depends on the calculated temperatures (Eq. 1) and the wavelength of interest. This flux density is then scaled by a dilution factor proportional to D^2/Δ^2, where D is the diameter, and Δ is the *Spitzer*-centric distance. The phase angle, which is invariably very small for KBOs, enters into the integral over the visible hemisphere. Here we have set $\alpha = 0$, as the effects are negligible for the actual phase of our observations ($\alpha = 1.86°$). The total flux density thus depends on both the target's unknown diameter, D, and albedo, p_V, as well as its distance from the Sun and the observer. Solutions for the size and albedo require a second equation; the object's visible magnitude typically provides this constraint. We used the absolute visual magnitude of Doressoundiram *et al.* (2005), $H_V = 5.37$, to relate the diameter and albedo via $D = 10^{-H_V/5}1329/\sqrt{p_V}$ (*e.g.,* Harris 1998), where D is the diameter in km.

The 24 and 70 μm photometry and results from the STM thermal model are shown in Figure 2a. Using the values of q and ϵ noted above, we allowed η to vary. The best fit to the

data in Figure 2a has $D = 420$ km, $p_V = 0.073$, and $\eta = 1.2$. The range of model parameters that are consistent with the 1σ error bars of our data are summarized in Table 3. We note that the model parameters are the *system-average, or effective, values of the diameter, albedo, and beaming parameter*, because the system is not resolved at 24 nor 70 μm (nor at V for the ground-based visible measurements). It is not unusual to allow η to range above unity (Harris 1998; Fernández et al. 2003; Delbo et al. 2003) when fitting thermal data with the STM. As can be seen from Equation 1, $\eta > 1$ will result in overall lower surface temperatures, even though η was traditionally introduced to model elevated localized temperatures caused by roughness. We interpret $\eta > 1$ to be an indication that the body has a non-zero thermal inertia, a relatively short rotation period, a fairly smooth surface, or some combination of the three. Therefore, the idealized assumptions in the STM do not perfectly apply. This is not entirely surprising given the low temperature of the object, which has the effect of lengthening the radiative cooling timescale, violating the instantaneous thermal equilibrium assumption of the STM.

The Isothermal Latitude Model (ILM) is the opposing end-member model to the STM: the target is assumed to have a surface with infinite thermal inertia, or, equivalently, to rotate instantaneously (also called the "fast-rotator model"; Lebofsky & Spencer 1989). In real terms, the ILM applies for objects with rotation periods much shorter than the timescale for radiative cooling of the surface. It is also typically assumed that the subsolar latitude is zero, although other geometries can be readily computed. In this geometry the surface temperature depends only on the latitude, and is constant over longitude. Strictly speaking, under the ILM $\eta = 1$.

Figure 2b compares our photometry with ILM models. We were unable to fit the data under the assumption that $\eta = 1$, and so again allowed it to be a free parameter. The resulting best fit has $D = 401$ km, $p_V = 0.080$, and $\eta = 0.44$. The range of model parameters consistent with our data are summarized in Table 3. We interpret $\eta < 1$ under the ILM as an indication that the thermal inertia could actually be rather low (although the STM results indicate that it is very likely greater than zero).

If the orientation of the rotational axis and the rotational period are known, it is possible to improve the ILM model results by accounting for the actual viewing geometry. Such a tilted ILM is an end-member case of a thermophysical model, incorporating the time-dependence of insolation, conduction, and re-radiation. If we assume that the rotational axes of the (47171) 1999 TC_{36} binary components are approximately aligned with the orbit normal, the viewing geometry of our observations is specified. Using the position of the normal to the (47171) 1999 TC_{36} orbit (Margot *et al.* 2005b), we find that the sub-*Spitzer* and sub-Solar latitude was $\simeq 49°$. Table 3 summarizes the results of the ILM for this

geometry.

Using the same assumption for the orientation of the rotation axes, we also fit the data using a smooth-surface thermophysical model, which includes the time-dependent effect of conduction into and out of the subsurface (*e.g.* Spencer 1990). The results in terms of p_V, D, and thermal inertial, Γ, and for assumed rotational periods of 10 and 40 hours are summarized in Table 3. The spectral energy distributions resulting from these models are nearly indistinguishable from those shown in Figure 2. Also, because we have added a model parameter, somewhat larger ranges of p_V and D are found to be consistent with the data.

We also undertook a Monte Carlo approach to see if we could constrain the pole orientation of (47171) 1999 TC_{36}. In this case we used the rough-surface thermophysical model of Spencer (1990). Thermal inertias (5 – 100), emissivities (0.9 – 1.0), albedos (0.01 – 0.5), rotational periods (6 – 32 hr), and spin orientations were all varied randomly (within the ranges just given); the spin orientation was distributed homogeneously in terms of solid-angle with respect to the line of sight. Parameters from thermophysical models with 24 and 70 μm fluxes consistent with our data and the absolute V magnitude for (47171) 1999 TC_{36} (to within $\pm 1\sigma$) were tabulated. Of the 300000 models we ran, 539 were consistent with the observations. The results of this modeling are shown in Figure 3. While a significant range of model parameters are consistent with our thermal measurements, clustering of the points shows that some portions of the parameter space are more likely than others. Acceptable models had geometric albedos between 0.052 and 0.108, and effective diameters between 340 and 483 km, entirely consistent with the ranges of those parameters found earlier, and confirming that those ranges encompass uncertainties resulting from model assumptions.

Interestingly, thermophysical models with very high ($> 70^\circ$) or with very low ($< 24^\circ$) sub-solar latitudes could not fit the data. 80% of the fitting models have sub-solar latitudes between 40° and 60°, neatly bracketing the 49° implied by alignment between the spin-axis and the satellite orbit angular momentum vector. Tidal evolution frequently drives satellite spins towards zero obliquity (Peale, 1999), but the obliquity of the primary is relatively insensitive to tidal evolution under the influence of the satellite. If the (47171) 1999 TC_{36} binary formed in a massive impact (similar to the Pluto-Charon forming impact, Canup 2005) the angular momenta vectors of the orbit and primary rotation should be nearly parallel. Other mechanisms proposed for forming Kuiper Belt binaries do not appear to predict any particular relationship between the orientation of spin and orbital angular momenta (Weidenschilling 2002; Goldreich *et al.* 2002; Funato *et al.* 2005). If our prediction that the spin of the (47171) 1999 TC_{36} primary is roughly aligned with the orbital angular momentum could be independently verified (or disproved), it would help constrain how the binary formed in the first place.

The rough-surface thermophysical models suggest that $\Gamma > 30$ J m^{-2} K^{-1} s$^{-1/2}$ for (47171) 1999 TC$_{36}$. Many of the best fitting models are clustered at the upper end of the range of Γ we explored (see Figure 3), so it is possible the thermal inertia is greater than the upper limit of 100 which we imposed. Some models that are consistent with the data also have Γ as low as 7.5, but are associated with improbable combinations of the other model paramters. Γ is around 50 for the Moon, and in the range 15 – 100 in these units for Pluto (Lellouch *et al.* 2000). Cruikshank *et al.* (2004) estimated Γ for 2002 AW$_{197}$ to be below 20, for an assumed equatorial viewing geometry. As the geometry moves to higher latitudes the effect of thermal inertia is diluted (in the extreme case, a pole-on ILM is quivalent to the STM, and no constraint can be placed on Γ). These values of Γ are consistent with a porous or particulate surface, or the presence of a low-conductivity material such as amorphous water ice or unconsolidated carbonaceous particles in the surface layers.

From all of these model fits to the data, we find that the effective diameter of the (47171) 1999 TC$_{36}$ system is in the range $350 < D < 470$ km, and the visible geometric albedo in the range $0.055 < p_V < 0.11$. These adopted values (Table 3) encompass both measurement uncertainties on the fluxes, and the uncertainties associated with interpreting the fluxes using the suite of thermal models described above. Because the only common outputs of all the models are albedo and size, we only provide adopted values for those quantities. These parameter ranges exclude some of the most extreme models that fit the data, but span most of the reasonable models. It further appears that the surface has a thermal inertia large enough to result in non-zero night-side temperatures, but that diurnal temperature variations are also likely to be important. For STM models, this is evidenced by the necessity to set η to values greater than unity, while for ILM models we have to set it to values around 0.5 (see Table 3). The thermophysical models confirm that (47171) 1999 TC$_{36}$ has a temperature distribution intermediate between the STM and ILM, with thermal inertia between about 30 and 100 J m^{-2} K^{-1} s$^{-1/2}$.

2.2. Comparison with sub-millimeter results.

Altenhoff *et al.* (2004) used the 30 m IRAM mm telescope to measure the 1.2 mm flux density from (47171) 1999 TC$_{36}$ as 1.1 ± 0.26 mJy. They used the ILM with $\eta = 1$ to interpret their data, and derived diameter and albedo values of $D = 609$ km (562 – 702 km), and $p_V = 0.05$ (0.04 – 0.06). Extrapolating our STM and ILM models to 1.2 mm we predict the flux density there to be 0.6 ± 0.16 mJy, or 55% of their observed flux, although our 1σ upper bound of 0.76 mJy is not far from their 1σ lower bound of 0.84 mJy. A similar discrepancy exists between the *Spitzer* results for (55565) 2002 AW$_{197}$ (Cruikshank *et al.* 2004) and the

sub-mm results reported by Margot *et al.* (2002), although the disagreement in the case of (47171) 1999 TC_{36} is somewhat worse.

The Altenhoff *et al.* data for (47171) 1999 TC_{36} were taken in queue mode in several epochs during the winter months of 2001 – 2003. Their errors include a 15% absolute calibration uncertainty, and an 18% uncertainty based on the measured noise in the data. When data from all epochs are stitched together, the signal integrates upward smoothly, in-spite of being obtained in such a distributed way: there is nothing within the data set to suggest that there is an issue (W.J. Altenhoff, *priv. communication*). Nevertheless, it seems possible that combining data from so many epochs might contribute to errors higher than nominal, so perhaps the discrepancy with our data can be attributed to somewhat optimistic error estimates for the 1.2 mm data. If irreconcilable differences between sub-mm measurements and Spitzer measurements turn up for additional distant solar-system objects, a coordinated effort to compare the two calibrations may be called for.

2.3. Component diameters.

Given the constraints of the observed magnitude difference of the pair, Δm, from Margot *et al.* (2004; 2005b, and Table 1) and total brightness consistent with our values for the effective diameter and albedo for the system, some limits can be inferred on the sizes of the components of (47171) 1999 TC_{36}. Figure 4 shows the combinations that satisfy these constraints for $D = 405$ km and $p_V = 0.079$ (these same basic curves are traced-out for other values of D and p_V, they simply extend to somewhat larger or smaller values of D). Assuming that the components have equal albedos, the ratio of their diameters in terms of their observed magnitude difference is $(d_1/d_2)^2 = 10^{\Delta m/2.5}$, where d_1 is the radius of the primary. Given the effective diameter, D, of the pair from our thermal results, the diameter of the primary is $d_1 = D/(1+(d_2/d_1)^2)^{1/2}$, and d_2 is found from the previous equation. Taking $D = 405$ km, the sizes of equal-albedo components are 379 and 133 km. An alternate case is that the 2 components have diameters equal to $0.5D$, and the apparent brightness difference is entirely due to an albedo difference. In this case the above expressions can be re-written to show that the albedos of the primary and companion are 0.28 and 0.039, respectively. The most extreme sizes that are allowed are $d_1 = D = 405$ km (in which case $p_{V1} = 0.069$), and $d_2 = 40$ km (in which case $p_{V2} = 1$). An albedo of 1 is probably quite unrealistic for a smallish KBO: a more reasonable upper limit might be $p_{V2} = 0.4$, in which case $d_2 = 66$ km. The data collected by Margot *et al.* (2005b) were unsuitable for making the difficult measurement of the mass ratio, but knowledge of that ratio would provide another useful constraint on the sizes of the components, and thereby improve our density determination (as discussed

below). In summary, for our best effective diameter, $D = 405$ km, the component diameters seem likely to lie in the ranges $202.5 \leq d_1 \leq 405$ and $202.5 \geq d_2 \geq 66$.

3. Density

Given the mass determined by Margot *et al.* (2004; 2005a; 2005b) and our determination of the effective diameter of the (47171) 1999 TC_{36} pair, the system density in terms of the sizes of the primary and companion is

$$\rho = \frac{6M}{\pi D^3} \frac{(1+\Delta_2)^{3/2}}{1+\Delta_2^{3/2}}$$

where M is the system mass, $\Delta_2 = 10^{-\Delta m/2.5} = d_2^2/d_1^2$, and other quantities are as defined earlier. Due to the D^3 term, the error in our determination of the size of (47171) 1999 TC_{36} strongly dominates the error in the mass in determining the uncertainty in the density. Table 4 summarizes the resulting densities for our adopted range of D and p_V, and for the range of component diameters discussed above. Considering the densities that result from the entire suite of model parameters, we adopt $\rho = 0.5$ g/cm^3 as our best estimate of the density, with the true value likely to fall in the range 0.3 – 0.8 g/cm^3.

Very low densities have been determined for many primitive solar system objects, in particular small bodies. For example, Asphaug and Benz (1996) estimated the density of comet Shoemaker-Levy 9 to have been 0.6 g/cm^3 based on observations of its tidal break-up during a close encounter with Jupiter. Three main-belt asteroids with diameters $>$ 100 km have densities < 1.5 g/cm^3 (15 Eunomia, 45 Eugenia, and perhaps 90 Antiope). Of these, Eunomia is particularly interesting because its density (0.96 ± 0.3 g/cm^3) is far below the average density for S-class (stony) asteroids (2.7 g/cm^3), and because it is the largest asteroid (diameter 255 km) with such a low density (see Britt *et al.* (2002) and Hilton (2002) and references therein). Anderson *et al.* (2005) find that the density of Jupiter's moon Amalthea (diameter $\simeq$ 83 km) is 0.86 ± 0.2 g/cm^3. Margot and Brown (2001) discovered that 87 Sylvia was a binary, and using the IRAS diameter derived a density of $\simeq 1.6$ g/cm^3. Marchis *et al.* (2005) subsequently discovered that Sylvia is actually a triple asteroid (the first known, with two satellites orbiting the primary), and estimated the density of the $\simeq$ 150 km diameter primary be 1.2 ± 0.1 g/cm^3. Trilling and Bernstein (2005) applied rotational stability arguments to the 33 KBOs and Centaurs with published lightcurves and show that none require densities larger than 0.5 - 1.5 g/cc (for various models) to remain gravitationally bound given their observed rotation rates. While this does not mean their densities are in that range (higher densities are not ruled out), it is interesting to note that the low density we find for (47171) 1999 TC_{36} is in accord with the lower-end of their limits.

Because the rotation period of (47171) 1999 TC_{36} is unknown, their analysis can not be directly applied to it (although such an analysis could be very revealing).

It is relatively easy to imagine strength-dominated objects less than around 200 kilometers across having very low densities (and presumably high porosities). Most of the low-density objects just mentioned are known to have irregular shapes (see references given above), indicating material strength does indeed dominate gravity in their interiors. Such densities could be achieved via catastrophic disruption and re-accumulation (*e.g.* Richardson *et al.* 2002). Such configurations are far less intuitively appealing in the case of an object such as (47171) 1999 TC_{36}, likely to be more than 300 kilometers in diameter, in which gravitational forces are likely to dominate material strength for some significant portion of the interior.

3.1. Interior Structure.

Given an assumption for the density, ρ_0, of the material making up the solid portions of (47171) 1999 TC_{36}, the fractional void space, or porosity, f, can be calculated from the total mass and the component diameters as $f = 1 - \rho/\rho_0 = 1 - (6M)/(\pi(d_1^3 + d_2^3)\rho_0)$. Plausible values for ρ_0 range from around 0.9 g/cm^3 (that of water ice, almost certainly the dominant constituent (*e.g.* Anders & Grevesse 1989), and other molecular ices likely to be present) to that of Pluto and Triton (2 g/cm^3, McKinnon *et al.* 1997), which are composed of roughly equal mass fractions of water ice and "rocky" material. Pluto is a particularly likely compositional surrogate for (47171) 1999 TC_{36}, because both bodies occupy the same orbital resonance with Neptune and so probably formed at a similar heliocentric distance (although (47171) 1999 TC_{36} has a lower orbital inclination, and so may have formed exterior to Pluto). While Pluto is differentiated, significantly compressed by its own gravity, and probably lost some icy material in a Charon-forming impact (Canup 2005) it is very difficult to imagine how (47171) 1999 TC_{36} could have formed with a significantly different rock fraction. That being said, our density for (47171) 1999 TC_{36} would be easier to accept if ρ_0 were near or even below 1 g/cm^3, suggesting a dearth of silicate materials, and a corresponding enrichment of water ice and other low-density molecular ices. Candidate ices other than water that might be somewhat abundant are CO (ρ = 1.0 g/cm^3), N_2 (ρ = 0.95 g/cm^3), and CH_4 (ρ = 0.5 g/cm^3) (Scott, 1976; Jiang *et al.* 1975; Manzhelii and Tolkachev, 1964). However, appealing to such an extreme composition is ad-hoc at best, and it seems highly unlikely that the low density can be explained without significant internal porosity or some other effect.

Figure 5 shows the porosity we derive for (47171) 1999 TC_{36} for the plausible range of

material densities, and for our adopted range of effective diameter for the system. Porosity values for selected values of ρ_0 are given in Table 4. If we assume the material density is $1.2 < \rho_0 < 1.8$, then for an effective diameter of 405 km the range of porosity required is about 62 – 74%. If we take 1.5 g/cm^3 as a likely average material density, then our adopted size limits constrain the porosity to be between 48 – 80%. Porosities in the range 45 – 80% cover most of the allowed values in Figure 5. If we take $D = 609$ km from from Altenhoff *et al.* (2004) and set $\rho_0 = 0.8$ g/cm^3, the porosity is 83%, and it gets progressively higher for larger material densities. We conclude that our results, if interpreted in terms of void spaces internal to (47171) 1999 TC_{36}, require the porosity to be about 65%, with a range of about 45 – 80%. It is astonishing to think of such a large body having more than half of its interior volume taken up by voids. Such an object strains the bound of what might reasonably be called a "rubble-pile" (Weissman 1986), being volumetrically more akin to a "void-pile", with some solid matter thrown in.

Our lower porosity limit, 45%, is still well in excess of the 26% expected for closely-packed equal-sized spheres, and is also in excess of that expected for randomly-packed equal-sized spheres (36%, *e.g.* Torquato *et al.* 2000). If the component pieces are unequal, porosity decreases because the smaller ones will infill the gaps between the larger ones. An important effect that increases the porosity of a collection of particles is friction, which could be due to roughness and/or angularity of those particles. Thus, a model which might be consistent with the high porosity implied by our density measurement is that the rubble in the interior of (47171) 1999 TC_{36} be both very irregular and of comparable size. Another could be that the rubble is itself porous. Such a configuration might result from relatively gentle assembly of grains to make macro particles, which then assemble to form porous "boulders", and so-on until a large object with significant porosity at all scales results. Similarly, sublimation of volatile components from within a water ice matrix could result in porosity at multiple scales. However, such paradigms ignore the fact that considerable momentum and energy must be dissipated during accretion, because accreted material will be deposited *via* high-velocity impacts. Such impacts will lead to local compression, melting, and vaporization, and in some cases large-scale fracturing (*e.g.* Asphaug *et al.* 1996; Richardson *et al.* 2002). Indeed, impacts would generally tend to compress such a porous structure as that discussed above, casting doubt on whether it could arise during accretion or be maintained during subsequent billions of years of cratering.

(47171) 1999 TC_{36} is also large enough that the expected internal stresses should lead to crushing and densification in the interior. The stress at the center of a homogenous sphere is $P_0 = \pi G \rho^2 D^2/6$. Taking the highest-pressure scenario for (47171) 1999 TC_{36} we set $\rho = 1$ (somewhat above the top of our range for density) and $D = 405$ km and find $P_0 = 6 \times 10^7$ dyn/cm^2. The yield strength of water ice is 10^7 dyn/cm^2 (Beeman, 1988)

at low confining pressures. In the case of a rubble-pile object, the confining pressure is essentially zero (*i.e.* the entire weight of overburden is comparable to the deviatoric stress at contact points between the fragments), and the low-pressure strength is the relevant one. So if the density of (47171) 1999 TC_{36} were around 1 g/cm^3 and the primary were as large as our best-fit effective diameter for the system, voids in the deep interior would indeed be closed via crushing of icy material. However, P_0 depends on the square of both the density and the radius, so modest reductions in either or both lead to significant reduction in interior stress. For a density of 0.5 g/cm^3 and a diameter of 300 km, $P_0 = 8 \times 10^6$ dyn/cm^2. It appears that (47171) 1999 TC_{36} may be on the verge of being large and dense enough that it would be compressed, at least near the center, by its own weight. If so, and if the density of larger KBOs can be measured, we predict that the larger objects would indeed have to be denser.

The finding that significant strength-supported void space could exist in the interior of (47171) 1999 TC_{36}, is still somewhat puzzling. The lack of a lightcurve greater than 5 – 10% (Peixinho *et al.* 2002, Ortiz *et al.* 2003; Margot *et al.* 2005a) is itself evidence that gravity dominates strength in the interior, resulting in the relaxation of meso-scale topography and a near-spherical shape. To explore this apparent inconsistency, we examined the possibility that (47171) 1999 TC_{36} has a low density (porous) outer mantle, and a denser, non-porous core. Such a configuration might arise in an impact that produced a largest fragment that was a significant fraction of the size of the original body, as would be expected from a collision with a specific energy at or somewhat above the shattering specific energy, Q^* (*e.g.* Holsapple *et al.*., 2002). Figure 6 shows results for the average density and porosity of (47171) 1999 TC_{36} as a function of the size of a hypothetical core. The figure assumes that the core is composed of a rocky component, with densities taken from the McKinnon *et al.* (1997 and references therein) models for the composition of Pluto, and that the density of the mantle is 0.5 g/cm^3 (consistent with a composition dominated by water-ice with about 50% porosity). The upper-limit on the density of the binary, 0.8 g/cm^3, places only a weak constraint on the size of a rocky core within (47171) 1999 TC_{36}: it could be as large as 0.45–0.51 of the total radius (depending on the core composition) and still satisfy our upper-bound on the density of (47171) 1999 TC_{36}. If the density is really 0.5 g/cm^3, there can be no core unless the mantle density is still lower. Setting the mantle density to 0.3 g/cm^3(*i.e.* setting its porosity to 70%), we find that a rocky core could exist within (47171) 1999 TC_{36} but that its size would be limited to 0.40–0.45 of the total radius. These results offer a compromise wherein (47171) 1999 TC_{36} has a relatively dense core overlain by a very porous, water-ice mantle. The sperical shape of the core would presumably help to moderate the external form, causing the overall shape to tend towards the sphericity suggested by the lack of a measureable lightcurve.

In summary, while the nominal density and porosity we determined above are not strictly inconsistent with considerations of cosmochemistry, formation, evolution, and strength *vs.* gravity, in each of these areas it seems that our nominal density range (0.3–0.8 g/cm^3) is extreme. The tolerance of our density for the presence of a high-density core, even if that core is dominated by silicates with densities around 3 g/cm^3, provides for a plausible scenario where (47171) 1999 TC_{36} can have a low-density/high-porosity and also have a spherical shape. However, such a low density for such a large object is still extreme.

3.2. Multiple System?

An alternative to the porous/rubble-pile models above is that one or both components of (47171) 1999 TC_{36} are very irregular in external form, essentially incorporating significant void space within their apparent limbs. As just discussed, this seems unlikely because of the lack of a measured lightcurve. However, an extreme case of such external porosity would be if one or both of the two known components are also binary (or multiple) systems. Three multiple minor-planet systems are known: 87 Sylvia is a triple (Marchis *et al.* 2005), Pluto is a quadruple (Weaver *et al.* 2005; Buie *et al.* 2005) and 2003 EL_{61} is a triple (Brown *et al.* 2005). If (47171) 1999 TC_{36} is a triple, the lack of a lightcurve is not particularly telling, as such a sub-binary would only possesses a lightcurve when one component eclipses the other (during mutual events), assuming the intrinsic lightcurve of each component is negligible. For a multiple system of N equal-size components, the density is given by $\rho = 6\sqrt{N}M/(\pi D^3)$: the density for the multi-component system is enhanced by a factor of $\sqrt{N}$ relative to that for a single component system. In the case of (47171) 1999 TC_{36} we postulate that the primary may itself be an unresolved binary with component diameters of d_1 and d_3; the diameter of the resolved companion to the primary is d_2, as before. If we restrict our consideration to the case where the three components have equal albedos, the density can be written as

$$\rho = \frac{6M}{\pi D^3} \frac{[(1+\Delta_2)(2+\Delta_3)]^{3/2}}{1+\Delta_3^{3/2}+\Delta_2^{3/2}(1+\Delta_3)^{3/2}}$$

where $\Delta_2 = d_2^2/(d_1^2+d_3^2)$, $\Delta_3 = d_3^2/d_1^2$. In addition, $\Delta_2 = 10^{-\Delta m/2.5} = 0.139$ from the observed magnitude difference between the primary and secondary.

Figure 7 shows the second term of the above expression as a function of the ratio d_1/d_3. From the figure it is clear that to have a significant effect on the density we derive, the primary must be split into components of comparable size. If the (47171) 1999 TC_{36} primary is actually 2 equal-sized components, this shows that the density of a trinary (47171) 1999 TC_{36} is enhanced by a factor of 1.60 relative to the density for a single-body, and 1.38 relative to the density of a binary sytem ($d_3 = 0$). The resulting average density of the triple

system is 0.7 g/cm^3, with a range of 0.4 – 1.1 g/cm^3 (compared to 0.3 – 0.8 g/cm^3 for the binary system). The porosities derived earlier decrease to about 0.5 with a range of 0.1 – 0.7. Table 4 summarizes our results for the density of this hypothetical trinary system. These densities and porosities might be achievable given the likely major constituents of (47171) 1999 TC_{36}, and realizable internal structures. Somewhat larger increases to the density could result if the secondary has a low albedo and is therefore comparable in size to the primary. In this case, and in the unlikely event that the secondary is also double, the density could be enhanced by a factor approaching 2 relative to the single-body density, or by a factor approaching 1.7 relative to the equal-albedo binary case.

4. Conclusions

We detected thermal emission from the binary KBO (47171) 1999 TC_{36} at 24 and 70 μm using the *Spitzer* space telescope. When interpreted using a range of thermal models, we derive an effective diameter for the system in the range $350 \leq D \leq 470$ km, with the best value being 405 km. The corresponding range of the visible geometric albedo is $0.055 \leq p_v \leq 0.11$, with the best value being 0.079. When combined with the system mass determined from HST data by Margot *et al.* (2004; 2005a; 2005b), our size determination indicates an average density in the range 0.3 – 0.8 g/cm^3. For likely bulk compositions, dominated by roughly equal mass fractions of rocky material and water ice, the porosity required to explain densities this low is in the range 55 – 75%. Such high porosities strain the bounds of what might reasonably be expected for naturally occurring internal structures for such a large object. However, we do find that (47171) 1999 TC_{36} is just small enough that it might not be compressed under its own weight, so porosities this high can not be easily ruled out on those grounds. It is possible that the (47171) 1999 TC_{36} primary could have a core with a density around 3 g/cm^3, so long as that core is smaller than about 1/2 the radius. The presence of a dense core may help reconcile the apparent inconsistency between the presence of large amounts of strength-supported void space in the interior and the nearly spherical shape evidenced by the lack of a measured lightcurve.

If (47171) 1999 TC_{36} is actually a triple system, the densities and porosities we derive must be modified accordingly. We derive a general expression for the density of the system as a function of the component sizes, and show that the density could actually be as much as 1.38 times greater than for the binary system, if the primary is split into comparably-sized components. Such a trinary system would be consistent with the lack of an observed lightcurve so long as none of the components eclipse one another (if the orbit of the primary-binary is inclined 49° to our line of sight, the centers of equal-sized components could be as

close as three radii without eclipses occurring). The density of such a system would be in the range 0.4 – 1.1 g/cm^3. At the upper end, these densities are comparable to that of, *e.g.*, Saturn's moons Tethys and Iapetus (*e.g.* Burns 1986).

These results suggest that in addition to being a binary KBO, (47171) 1999 TC_{36} has unexpected internal properties. The large model uncertainties in the density and porosity could be reduced with additional data that provided constraints on the individual sizes of the primary and secondary, or that constrained their individual masses. In addition, very high-resolution imaging or lightcurve monitoring could help resolve the question of whether the (47171) 1999 TC_{36} primary is itself actually multiple. If (47171) 1999 TC_{36} were found to have a short rotation period, that could place a lower bound on the density for which it would be stable against distortion or breakup due to rotation.

This work is based [in part] on observations made with the Spitzer Space Telescope, which is operated by the Jet Propulsion Laboratory, California Institute of Technology under a contract with NASA. Support for this work was provided by NASA through an award issued by JPL/Caltech.

REFERENCES

Altenhoff, W. J. *et al.* 2004, A&A 415, 771

Anders, E. and N. Grevesse 1989, Geochim. Cosmochim. Acta 53, 197.

Anderson, J.D. *et al.* 2005, Science 308, 1291

Asphaug, E. and W. Benz 1996, Icarus 121, 225

Astakhov, S.A. *et al.* 2005, MNRAS 360, 401

Beeman, M. 1998, JGR 93, 7625.

Boehnhardt, H. *et al.* 2001, A&A378, 653

Bowell, E., B. Hapke, D. Domingue, K. Lumme, J. Peltoniemi, & A.W. Harris 1989. "Application of Photometric Models to Asteroids," in *Asteroids II*, R.P. Binzel, T. Gehrels, M.S. Matthews, Eds. University of Arizona Press, Tucson.

Britt, D.T., E. Yeomans, K. Housen, G. Consomagno, 2002. "Asteroid Density, Porosity, and Structure." In *Asteroids III,* University of Arizona Press, Tucson, Arizona.

Brown, M.E. and C.A. Trujillo 2004, AJ 127, 2413

Brown, M.E. *et al.* 2005, ApJ *accepted*

Buie, M.W. *et al.* 2005, *submitted, astroph 0512491*

Burns, J.A. 1986. "Some Background on Satellites," in *Satellites*, J.A. Burns $ M.S. Matthews, Eds. University of Arizona Press, Tucson.

Campins, H. *et al.* 1994, AJ 108, 2318

Canup, R. 2005. A Giant Impact Origin of Pluto-Charon. *Science* 307, 546.

Cruikshank, D.P. *et al.* 2005. Protostars and Planets V (abstract).

Cruikshank, D.P. *et al.* 2004, ApJ 624, L53

Delbo, M., Harris, A.W., Binzel, R.P., Pravec, P., & Davies, J.K. 2003, Icarus 166, 116

Delsanti, A.C. *et al.* 2001, A&A380, 347.

Dole, H. *et al.* 2004, ApJS 154, 87

Dotto, E. *et al.* 2003, Icarus 162, 408

Doressoundiram, A. *et al.* 2005, Icarus 174, 90

Elliot, J.L., S.D. Kern, D.J. Osip, S.M. Burles 2001, IAU Circ. 7733

Fernández, Y. J. et al. 2002, AJ 123, 1050

Fernández, Y. J. *et al.* 2003, AJ 126, 1563

Funato, Y., J. Makino, P. Hut, E. Kokubo, D. Kinoshita 2005. The formation of Kuiper-belt binaries through exchange reactions. Nature 427, 518.

Goldreich, P. *et al.* 2002 Nature 420, 643

Gordon, K.D. *et al.* 2004, PASP 117, 503

Grundy, W.M. *et al.* 2005, Icarus 176, 184

Harris, A.W. 1998, Icarus 131, 291

Hilton, J.L. 2002. "Asteroid Masses and Densities." In *Asteroids III,* University of Arizona Press, Tucson, Arizona.

Holsapple, K., I. Giblin, K. Housen, N. Nakamura, E. Ryan 2002. "Asteroid Impacts: Laboratory Experiments and Scaling Laws." In *Asteroids III,* University of Arizona Press, Tucson, Arizona.

Jewitt, D.C. and J. Luu 1993, Nature 362, 730

Jewitt, D., Aussel, H, & Evans, A. 2001, Nature 411, 446

Jiang *et al.* 1975, J. Chem. Phys. 62, 1201

Lazzarin, M. *et al.* 2003, AJ 125, 1554

Lebofsky, L.A., et al. 1986, Icarus 68, 239

Lebofsky, L. A, & Spencer, J. R. 1989, in Asteroids II, ed. R. P.Binzel, T. Gehrels, T., & M. S. Matthews (Tucson: Univ. Arizona Press) 128

Lellouch, E, R. Laureijs, B. Schmitt, E. Quirico, C. de Bergh, J. Crovisier, A. Coustenis 2000, Icarus 147, 220.

Lellouch, E., Moreno, R., Ortiz, J. L., Paubert, G., Doressoundiram, A., & Peixinho, N. 2002, A&A 391, 1133

Lisse, C. *et al.* 2005, ApJ 625, 139

Lumme, K. and E. Bowell, 1981, AJ 86, 1694.

Malhotra, R. 1993, Nature 365, 819

Manzhelii and Tolkachev, in Sov. Phys. Solid State 5, 2506-2510 (1964)

Marchis, F. *et al.* 2005, Nature 436, 822

Margot, J.L. and M.E. Brown 2004, BAAS 33, 1133 (abstract)

Margot, J. L. *et al.* 2002, BAAS 34, 871 (abstract)

Margot, J.L., M.E. Brown, C.A. Trujillo, R. Sari 2004, BAAS 36, 803 (abstract)

Margot, J.L., M.E. Brown, C.A. Trujillo, R. Sari, J.A. Stansberry 2005a, BAAS 37, 803 (abstract)

Margot, J.L. *et al.* 2005b, *in prep.*

McBride, N. *et al.* 2003, Icarus 161, 501

McKinnon, W., D.P. Simonelli and G. Schubert, 1997. "Composition, Internal Structure, and Thermal Evolution of Pluto and Charon." In *Pluto and Charon,* University of Arizona Press, Tucson, Arizona.

Millis, R.L. and K.B. Clancy 2003, IAU Circ. 8251

Noll, K.S. *et al.* 2002a IAU Circ. 7824

Noll, K.S. *et al.* 2002b IAU Circ. 7857

Noll, K.S. *et al.* 2002c IAU Circ. 8034

Noll, K.S. 2003, Earth, Moon and Planets 92, 395

Ortiz, J.L., P.J. Gutierrez, V. Casanova, A. Sota 2003, å 407, 1149

Papovich, C. *et al.* 2004, ApJS 154, 70

Peale, S.J. 1999. Origin and Evolution of the Natural Satellites, ARA&A, 37, 533

Peixinho, N., A. Doressoundiram, J. Romon-Martin 2002, New Astron. 7, 359

Richardson, D.C., Z.M. Leinhardt, H.J. Melosh, W.F. Bottke, E. Asphaug 2002. "Gravitational Aggregates: Evidence and Evolution." In *Asteroids III,* University of Arizona Press, Tucson, Arizona.

Rieke, G.H. *et al.* 2004, ApJS 154, 25

Scott, T.A. 1976, Phys. Reports 27, 157

Spencer, J.R. 1990, Icarus 83, 27

Stansberry, J.A. *et al.* 2004, ApJS 154, 463

Stephens, D.C. and K.S. Noll 2005, submitted, astroph 0510130.

Stephens, D.C. and K.S. Noll 2004, BAAS 36, 170 (abstract)

Stern, S.A. 2002, AJ 124, 2300

Tedesco, E. F., Noah, P. V., Noah, M, Price, S. D. 2002, AJ 123, 2056

Tegler, S.J. and W. Romanishin 2005, *submitted*

Torquato, S. *et al.* 2000, *Phys. Rev. Lett.* 84, 2064.

Trilling, D.E. and G. Bernstein 2005, AJ, *in press*

Trujillo, C.A., and M.E. Brown 2002, IAU Circ 7787

Veillet, C., J.W. Parker, I. Griffin, B. Marsden, A. Doressoundiram, M. Buie, D.J. Tholen, M. Connelley, M.J.Holman 2002, Nature 416, 711

Weidenschilling, S.J. 2002, *Icarus* 160, 212.

Weaver, H.A. *et al.* 2005. Nature *in press*

Weissman, P.R. 1986, Nature 320, 242

Werner, M. *et al.* 2004, ApJS 154, 1

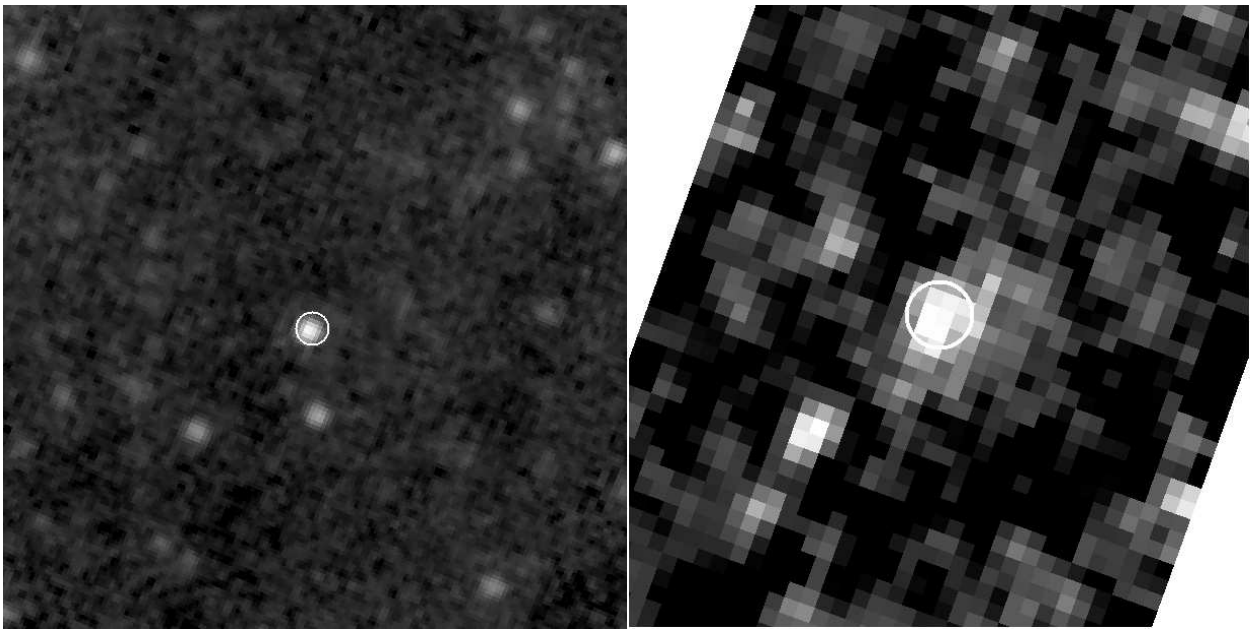

Fig. 1.— Images of (47171) 1999 TC_{36} at 24 μm (left) and 70 μm (right). Each image is 190″ square, and the orientation is North up, East left. The circles are centered at the ephemeris position of the target. It is just possible to make out the first Airy maximum in the 24 μm image. There is no significant background structure due to cirrus at either wavelength.

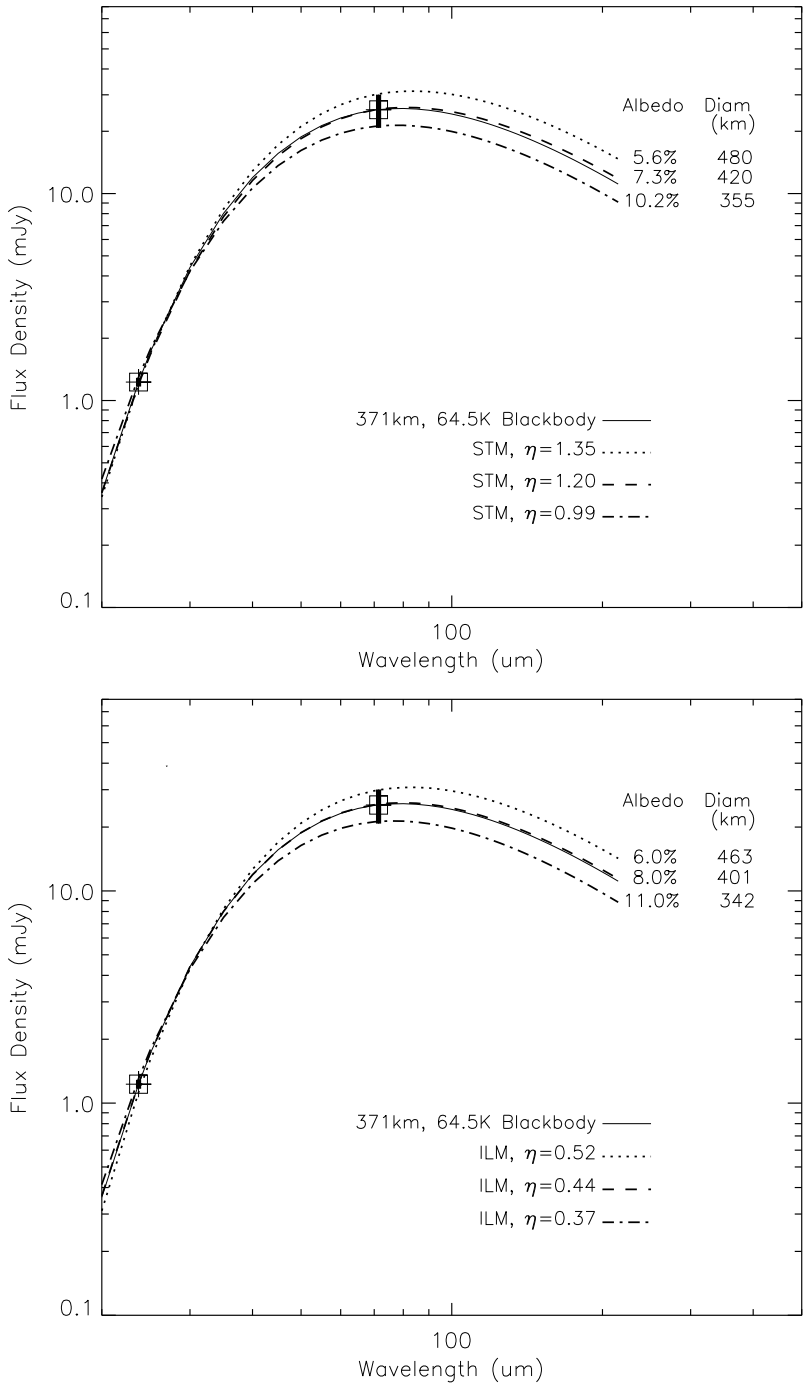

Fig. 2.— Thermal models fitted to our 24 and 70 μm photometry. Results from the Standard Thermal Model (STM) are given in panel a (top), and those from the Isothermal Latitude model (ILM) in panel b (bottom). Diameters, which are the effective total diameter for both components of the binary system, and effective geometric albedos corresponding to each model are given at upper right. The beaming parameter, η, for each model is given in the legend. The temperature of a zero-albedo surface at the distance of (47171) 1999 TC_{36} would be 70.6 K.

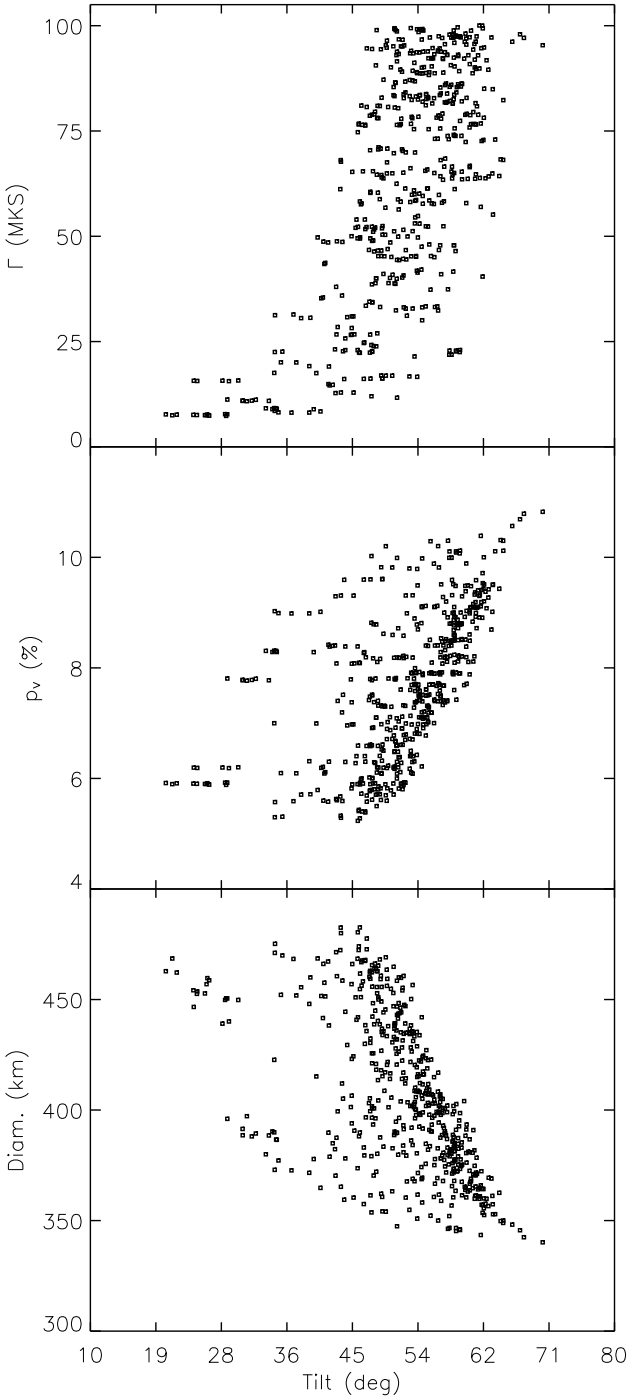

Fig. 3.— Model parameters for rough-surface thermophysical models consistent with our thermal photometry and the absolute V magnitude of (47171) 1999 TC_{36}. A point is plotted for each of the 539 models that fit the data (of 30000 models run).

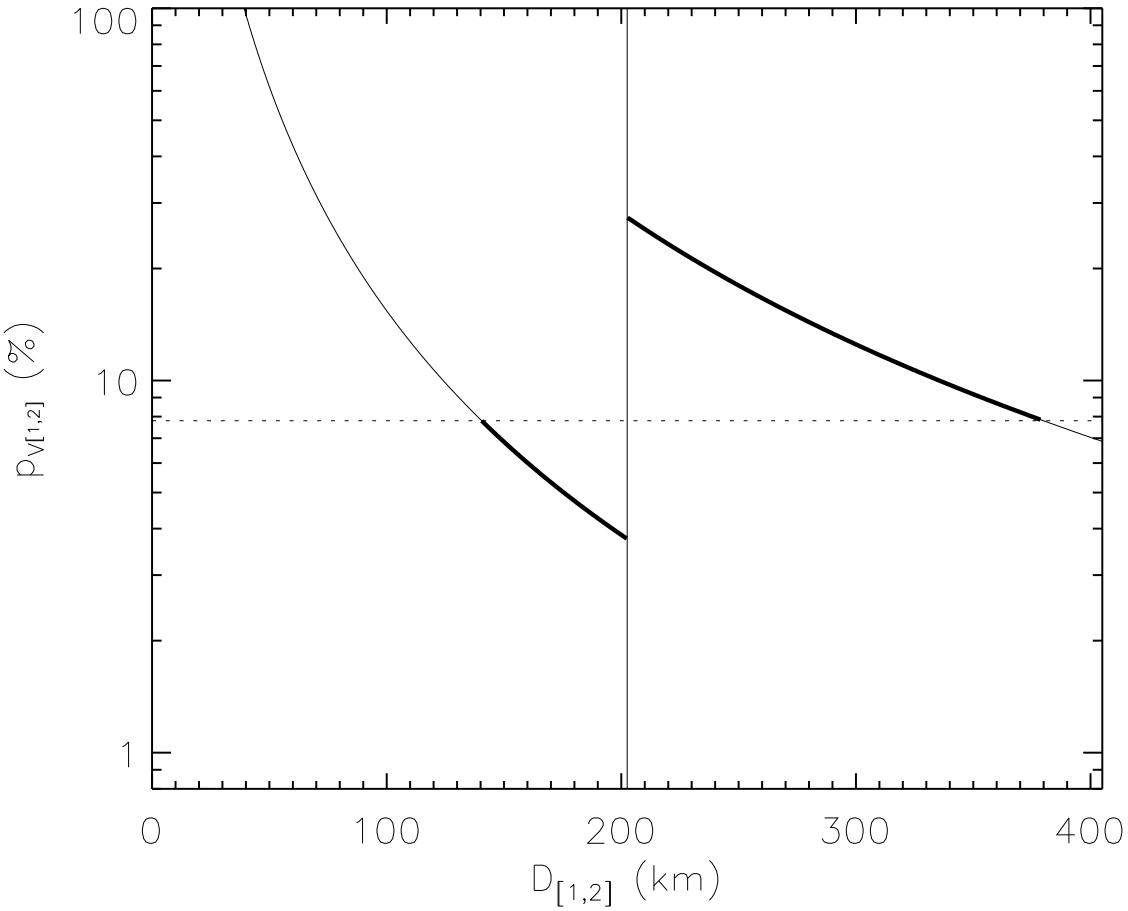

Fig. 4.— The locus of combinations of albedo and diameter for the (47171) 1999 TC_{36} primary (to the right of the vertical line), and companion. The solution shown applies for an effective system diameter and albedo of 405 km and 7.9%. The heavy lines show the range of solutions where the primary has a higher albedo than the secondary; the thin lines those ranges where the primary has a lower albedo than the secondary.

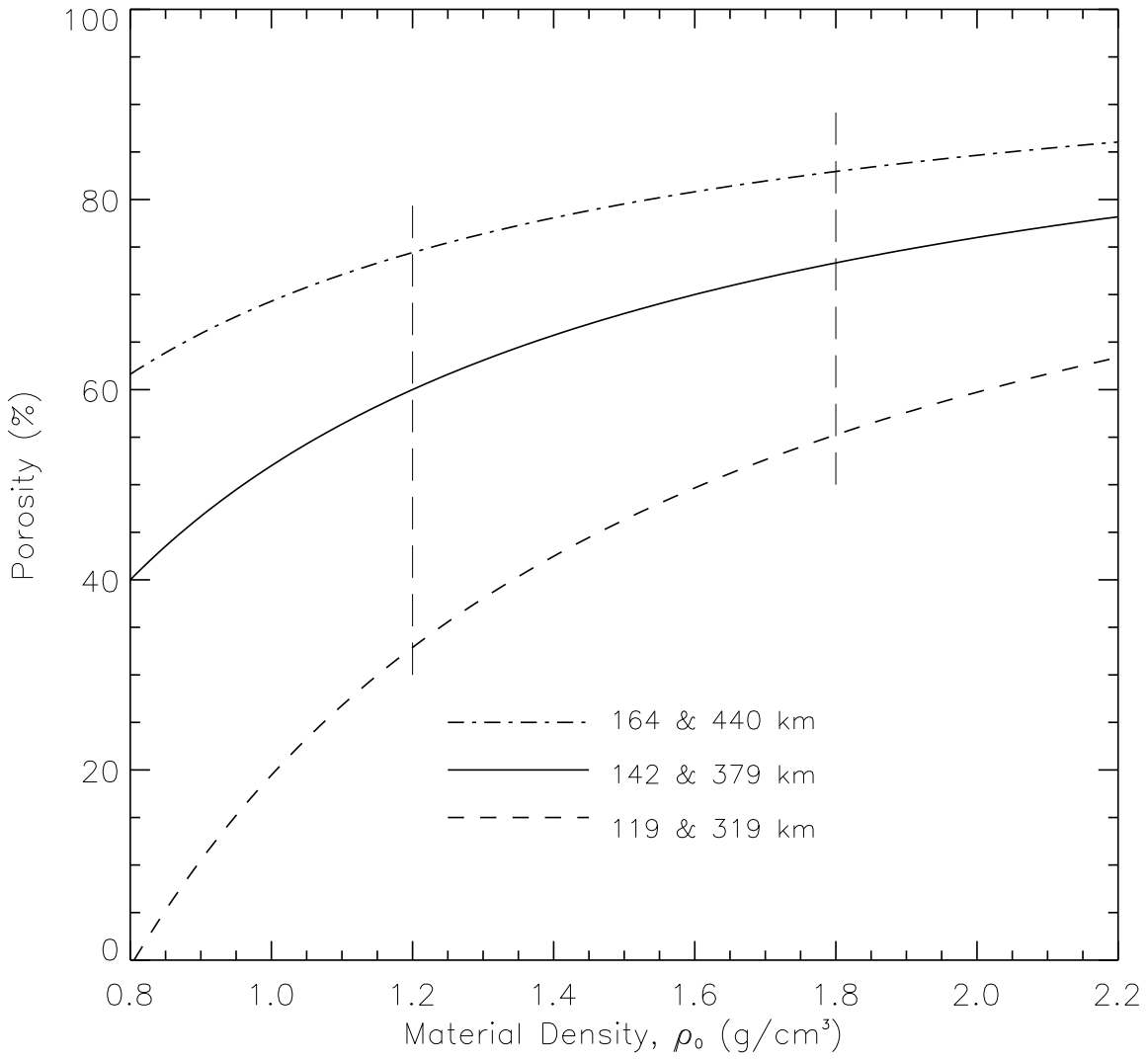

Fig. 5.— The fraction of void space within (47171) 1999 TC_{36} resulting from our determination of the effective diameter and the mass determination of Margot *et al.* (2005b). The 3 lines give the dependence for our adopted value (405 km) and limits (350 – 470 km) for the effective diameter. The legend gives the corresponding sizes of the components if they have equal albedos. The vertical lines indicate a reasonable range of material density in the outer Solar System (see text).

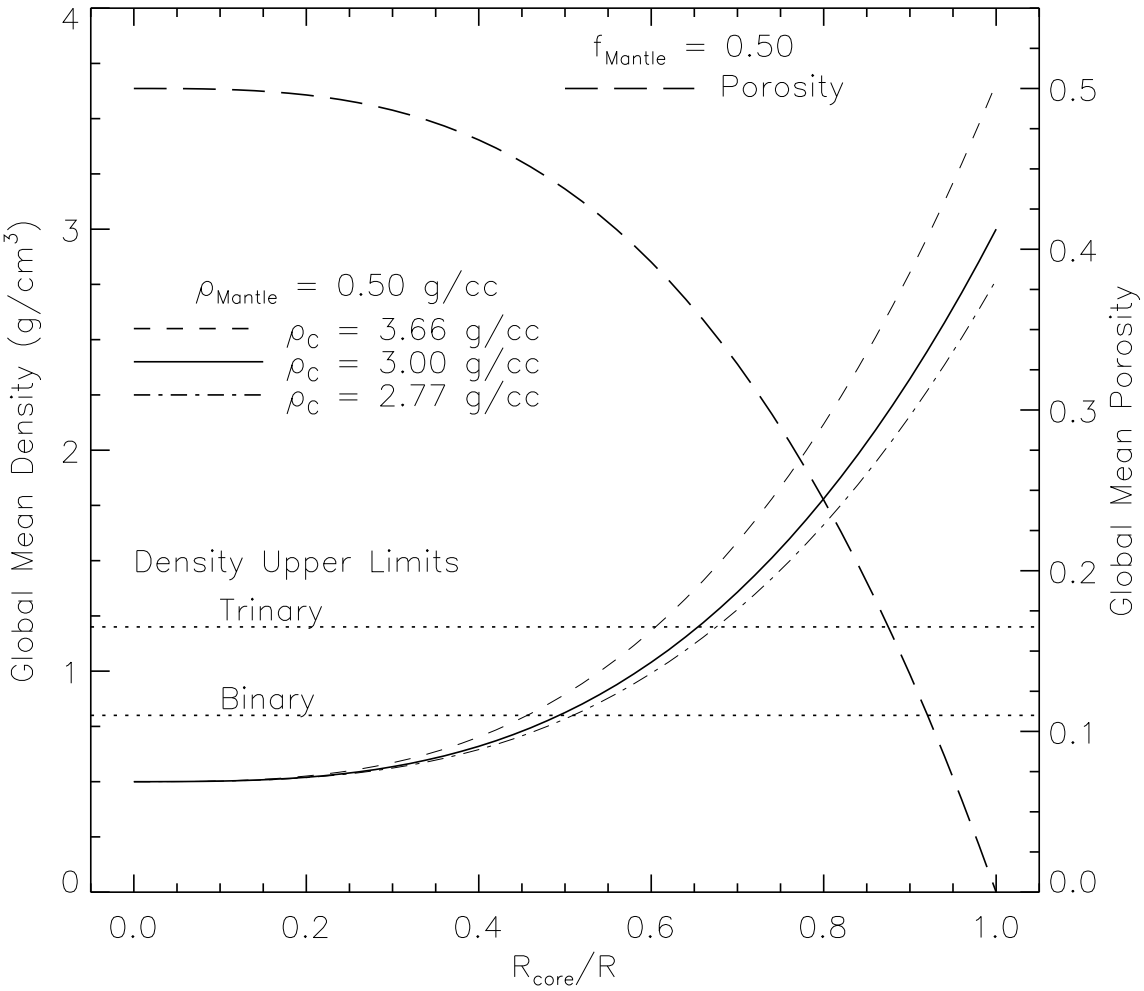

Fig. 6.— The density and porosity of (47171) 1999 TC_{36} as a function of the size of a hypothetical core. The density of the mantle (the layer surrounding the core) is taken to be 0.5 g/cm^3, consistent with a composition dominated by water ice with 50% porosity. The density of the material in the core (assumed to be dominated by silicates) is reflected by the legend labels ρ_C, with the resulting global mean density indicated by the corresponding linestyles. The average porosity of the entire 2-layer structure is given by the long-dashed line. Our upper limits on the density of binary and trinary versions of (47171) 1999 TC_{36} are shown as horizontal dotted lines. In spite of the high porosities required by our density, large non-porous cores with densities appropriate for rocky material are consistent with our data.

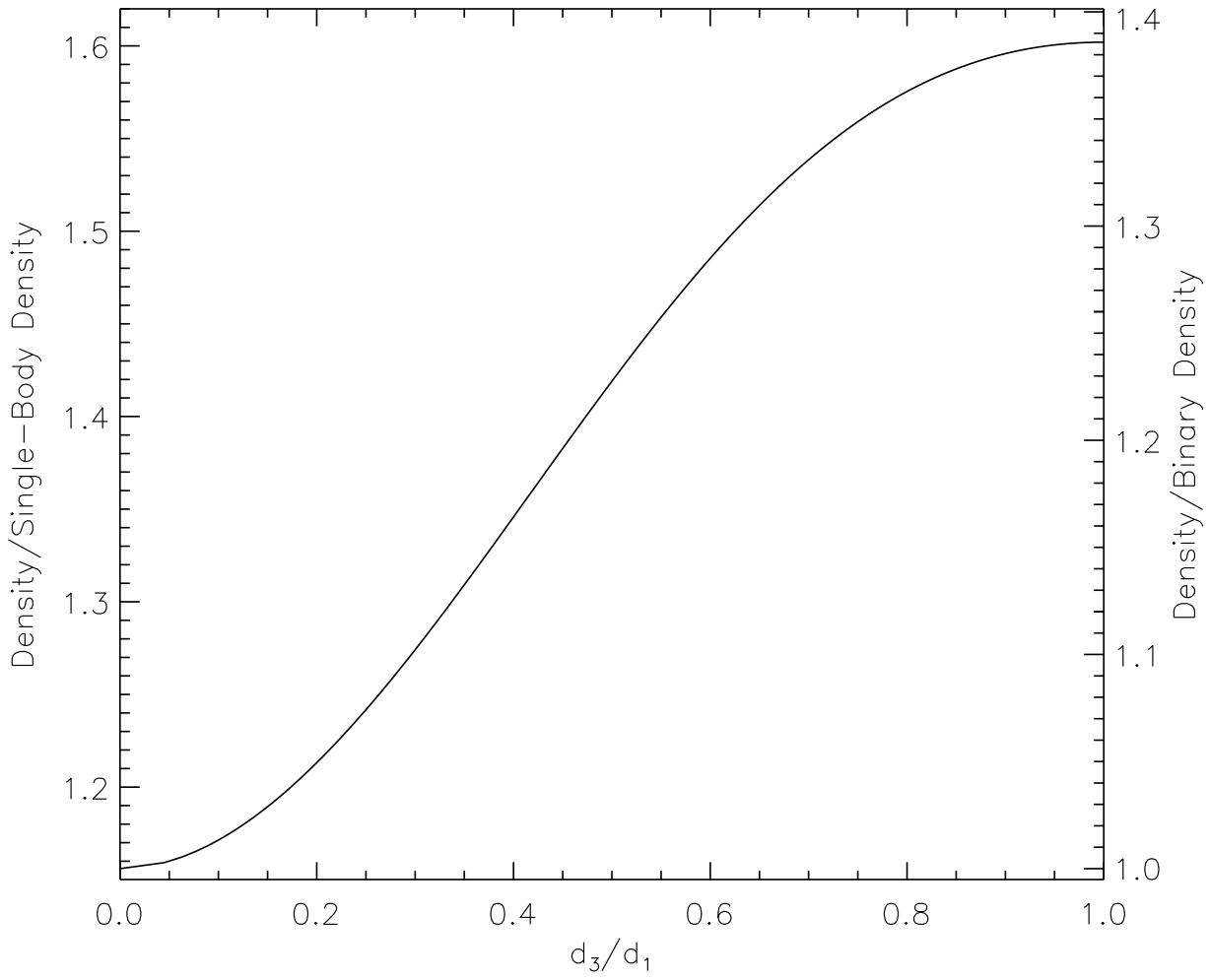

Fig. 7.— Density enhancement relative to the single-component system density ($6M/(\pi D^3)$) for a trinary system. The relationship shown assumes that all 3 components have the same albedo. For $d_3/d_1 = 0$ the system is a binary, and for $d_3/d_1 = 1$ the "primary" is itself a binary with 2 equal-sized components.

Table 1. The 1999 TC_{36} Binary System

Parameter	Symbol	Value
Heliocentric Orbit		
semi-major axis	A[a]	39.23 AU
eccentricity	e[a]	0.22
inclination	i[a]	8.4°
Binary System		
semi-major axis	a[b]	7720 km
system mass	M[b]	1.44×10^{19} kg
orbit period	P[b]	50.36 d
contrast	Δm[b c]	2.14 ± 0.02
size ratio	r_1/r_2[d]	2.68

[a]Heliocentric orbit values from the Minor Planet Center.

[b]Values from Margot *et al.* 2004; 2005a; 2005b. The uncertainty in the mass is about 15%.

[c]Visual magnitude difference between primary and secondary.

[d]Radius ratio of the components assuming equal albedos.

Table 2. Observational Circumstances and Flux Densities

Wavelength (μm)	Date[a]	Exposure (sec)	R_{Sun} (AU)	$\Delta_{Spitzer}$ (AU)	Flux (error) (mJy)
24	2004 Jul 12 10:41	1400	31.10	30.94	1.23 (0.06)[b]
70	2004 Jul 12 11:09	800	...	...	25.4 (4.7)[b]

[a]The J2000 pointing for the observations was 00:45:29.8, -04 16 59.

[b]Errors include those from the absolute calibration. The SNR of the detections was $\simeq 50$ at 24 μm, and $\simeq 10$ at 70 μm.

Table 3. Thermal Model Results

Model	D (km)[a]	p_V (%)[a]	η[a]	Γ[a c]
STM	420 (355 – 480)	7.3 (10 – 5.6)	1.2 (1.0 – 1.4)	0
ILM	401 (342 – 463)	8.0 (11 – 6.0)	0.44 (0.37 – 0.52)	∞
ILM (tilted)[b]	420 (364 – 488)	7.3 (9.7 – 5.4)	0.80 (0.7 – 0.95)	∞
T.phys. (10hr)[b]	434 (362 – 504)	6.9 (9.9 – 5.1)	...	3.5 (0.3 – ∞)
T.phys. (40hr)[b]	434 (362 – 504)	6.9 (9.9 – 5.1)	...	7.9 (0.7 – ∞)
Adopted	405 (350 – 470)	7.9 (11 – 5.8)	...	...

[a]Model results given as best value and (range).

[b]The tilted ILM and thermophysical models assumed a sub-solar and sub-*Spitzer* latitude of 48.6°.

[c]The units of Γ are $\mathrm{J\,m^{-2}\,K^{-1}\,s^{-1/2}}$.

Table 4. Density Results

Model	Density (g/cm^3)[a b]	Porosity[a b] ($\rho_0 = 1.2$ gcc)	($\rho_0 = 1.5$ gcc)	($\rho_0 = 1.8$ gcc)
Binary				
Equal p_v	0.48 (0.81 – 0.31)	0.59 (0.39–0.72)	0.67 (0.50–0.77)	0.71 (0.58–0.80)
Equal Size (D/2)	0.59 (0.99 – 0.37)	0.51 (0.26–0.68)	0.60 (0.40–0.73)	0.66 (0.49–0.77)
Max Difference	0.42 (0.73 – 0.27)	0.64 (0.45–0.75)	0.70 (0.55–0.80)	0.74 (0.62–0.83)
Adopted	0.5 (0.9 – 0.3)	0.53 (0.32–0.72)	0.65 (0.45–0.77)	0.69 (0.54–0.80)
Trinary				
Equal Size[c d]	0.69 (1.10 – 0.41)	0.43 (0.08–0.66)	0.54 (0.26–0.72)	0.62 (0.39–0.77)

[a]Results given as best value and (range).

[b]The values correspond to our adopted values for D, with further constraints as noted in the Model column.

[c]The trinary model assumes equal albedos for all 3 components. The primary is assumed to be 2 equal-sized components ($d_3 = d_1$).

[d]Trinary model values are based on the adopted binary densities and the density enhancement for $d_3 = d_1$.